NUMERICAL SIMULATION OF DENSIFICATION OF HETEROGENEOUS RANDOM POWDER PARTICLES WITH NON-EQUAL DIAMETER

K.P. Huang,[1,3] F.Z. Wang,[1] M.J. Zhao,[1] and Y.B. Wang[2]

This article builds the mathematical model of randomized 3D particles using a Python program to study the densification behavior of heterogeneous powder particles of non-equal diameter under pressure. The Python interface reserved by the finite element software Marc was applied to compile relevant command files and link them to carry out the numerical simulation of powder particle densification. The principles of particle distribution, deformation, and nodal flow were obtained by analyzing the powder particle compaction outcomes. The impact of particle parameters, compaction temperature, and coefficient of friction on the relative density of compacts was investigated. The results of the simulation show that the powder particles in the mould cavity are spiraling. Cu particles form concave arcs and cylindrical arcs at contact points, and the node trajectories rotate from top to bottom and from the center to the periphery. The overall deformation of Cr powder particles is not obvious. In the pressing process, the larger the powder particles, the greater the degree of deformity. As the temperature in the cavity increases, the relative density decreases. The higher the cavity friction, the higher the relative density, but once it reaches a certain value, the relative density reduces. The relative density of compacts can be greatly enhanced by selecting soft powder particles with a larger size, a higher temperature cavity, and a certain value of friction force. The experimental results verify the accuracy of the simulation, which is an important benchmark for numerical simulation of randomized particle densification. The findings provide a theoretical basis for further improvement in the density and properties of heterogeneous metal doping.

Keywords: *heterogeneous non-equal diameter, random particles, mathematical model, densification, numerical simulation.*

INTRODUCTION

Since the geometric features of the random arrangement of spherical particles are important in many technical fields, in particular in the field of powder metallurgy, the arrangement of binary powder particles within the cavity directly influences the properties of the sintered material [1, 2]. During powder particles compaction, the control of deformation is the principal factor to increase the density of the product. Due to the complexity and diversity of particle shapes, it is difficult to observe the law of deformation based on experiments. As a result, the

[1]Xi'an University of Architecture & Technology, No. 13 Yanta Road, Xi'an, Shaanxi Province, P.R. China.
[2]Zhuzhou Smelter Group Co., Ltd., 12 Hengshan East Road Tianyuan District Zhuzhou Hunan, Zhuzhou, Hunan, 412007, China.

[3]To whom correspondence should be addressed; e-mail: huangkp457@gmail.com.

filling of powder particles into the actual environment on the micro-level established. Numerical simulation of the model is of high importance when studying the densification process of powder particles [3–5].

In recent years, considerable progress has been made in investigating the influence of the pressing process on the deformation of powder particles. In the appearance of random stacking of powder particles and based on the method of discrete components of molecular dynamics, D.F. Wang systematically characterized and analyzed the topological and metric properties of the binary crystal structure by orderly stacking the generated binary crystal structure. However, the disordered stacking has not been under consideration [6]. Through the discrete element model established by Y.X. Zhang, a variety of initial packing structures of spherical particles with a single size were generated, including random stacking and miscellaneous ordered stacking, but the density of the arrangement could not achieve the actual suppression adjustment [7]. C. Li [8] conducted a systematic experimental physical study of the packaging and densification of binary spherical particles in one-dimensional and three-dimensional vibration conditions and achieved the densest packaging structure under various vibration conditions, but did not analyze the law of particle deformation. In terms of binary powder compaction, D.W. Wolla et al. [9] used the finite element method to successfully predict plastic fracture in Cu–Al powder metallurgy pre-forms but did not develop a theoretical filling model. Based on the theory of continuum mechanics and plastic deformation, Y. Zhang et al. [10] applied a constitutive porous ellipsoid yield model to perform finite element simulation of the Cu–Cr25 powder hot isostatic pressing process but did not analyze particle rheology. S. Zhao et al. [11] investigated the effect of particle strain size and particle friction factor on relative density under different compressive loads. However, they did not analyze it from a three-dimensional point of view. H.P. Chen et al. [12] examined the densification law of the W–Cu billet during the hot isostatic compaction process and determined the orthogonal optimization scheme for holding temperature, holding pressure, and holding time using the cross-test method, but fail to obtain the law of deformation of a single particle. As for the densification of Cu–Cr powder, Q.X. Liu et al. [13] performed a numerical simulation of the macrosegregation and temperature field of Cu–Cr binary alloys, without considering the friction effect between the particles. Y.B. Wang et al. [14] examined the effects of different compaction methods and the friction coefficient of Cu–Cr powder particles on changes in their density and morphology during unidirectional and bidirectional densification. Also, the rheological behavior of the particles of the three-dimensional model has been considered. However, this model is an orderly and regular arrangement and does not account for the disordered arrangement of particles under actual suppression. D.G. Wang et al. [15] discussed the density of bidirectional and unidirectional compaction regardless of the rheological behavior of the particles.

In summary, many experimental and theoretical results have been achieved in the study of metal powder densification at home and abroad, but all of them are based on macro- or micro-idealization research. However, there are few reports about the 3D microsimulation of randomly filling of Cu–Cr powder particles into a real environment. To provide a better explanation of the densification and uniformity of Cu–Cr powder particles in the pressing process, the computer programming language is used in this article to study binary powder particles and nodes within particles during the pressing process. The mathematical model of the random accumulation of powder particles in the mould cavity has been described. By analyzing the strain behavior and flow law of heterogeneous non-equal diameter random particles during the pressing process, we hope to have a deeper understanding of the densification behavior of Cu–Cr powder particles. The density and performance of heterogeneous metadoping have been improved to provide a relevant theoretical basis.

SIMULATION OF HETEROGENEOUS 3D RANDOM PARTICLES WITH NON-EQUAL DIAMETER

The actual filling process of the mould cavity must be considered in the construction of the 3D mathematical model of heterogeneous particles of unequal diameter. Given that the powder particles are affected by their own gravity, contact force and friction force between the particles and the cavity of the mould, and the intermolecular force between adjacent particles, the following assumptions may be made [16–18]:

1) The random morphology of heterogeneous powder particles of non-equal diameter is an ideal sphere, which is characterized by the coordinates of the sphere's center and the radius.

2) The contact surface of the particles with the cavity is very small compared to the spherical particles themselves, so they are all points of contact.

In order to perform a random collection of powder particles in the mould cavity, a random 3D mathematical model of powder particles is proposed and built by the Python program for the first time.

Prefilled Powder Particles. In the three-dimensional mold cavity, two powder particles with different radius are formed one by one in a 1 : 1 way into spheres, which are scattered adjacent and evenly stacked. Coordinate of the sphere center and a radius for the sphere to be generated shall be randomly specified, and an overlap judgment with all the spheres that were generated shall be made. If the distance from the center of the sphere to be generated to a sphere generated is less than the sum of the radii of the two spheres, the two spheres are regarded as overlapping. Otherwise, the coordinates of the spherical center are invalid, and it is necessary to further specify the coordinates of the spherical center.

Dynamic Adjustment. For random loosening of powder particles in the cavity, the coordinates of the sphere must be dynamically adjusted. Given the contact between the spheres, one of the spheres is selected as the target sphere on the move, and the remaining spheres are taken as reference spheres. Next, the geometrical relation between the position of the target sphere and the reference sphere before and after adjustment is taken into account.

Sphere A is the target sphere, sphere B is the reference sphere, and sphere C is the dynamically adjusted target sphere. Value $\vec{e}$ is the distance between the target and reference spheres, and a random direction vector $\vec{d}$ is defined in the coordinate system as the moving direction of the target sphere as shown in Fig. 1.

Thus, we obtain:

$$\vec{d} = (x, y, z) = (d \sin\alpha\cos\beta, d\sin\alpha\sin\beta, d\cos\alpha), \tag{1}$$

where α is the angle of $\vec{d}$ and z-axis; β is the angle of the projection $\vec{d}$ on the *xoy*-plane and the *x*-axis. By uniting the components on the *x*-axis, we get that:

$$\vec{d} = \left(1, \frac{y}{x}, \frac{z}{x}\right) = \left(d\cot\beta, \frac{\cot\beta}{\cos\beta}\right), \tag{2}$$

$$\vec{d} = \left(1, \cot\beta, \frac{\cot\beta}{\cos\beta}\right) = \frac{1}{\sqrt{1^2 + (\cot\beta)^2 + \left(\frac{\cot\beta}{\cos\beta}\right)^2}}. \tag{3}$$

Moving the target sphere along the selected direction $\vec{d}$ when it comes into contact with another sphere according to the law of cosines, we obtain:

$$r^2 = t^2 + \|\vec{e}\|^2 - 2t\|\vec{e}\|^2 \cos\theta, \tag{4}$$

where θ is the angle of the direction vector $\vec{d}$ and the binding direction of the two sphere centres; r is the sum of the radii of the two spheres; t is the offset before and after adjusting the coordinates of the target sphere center.
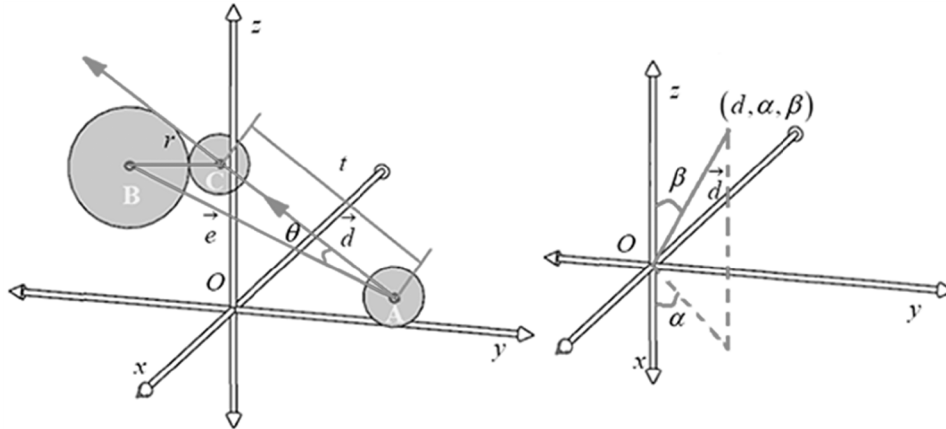

Fig. 1. Dynamic detection of geometric positions between spheres

The adjusted spherical center coordinates can be determined to solve this equation, so we can obtain:

$$t = \left(\vec{e} \cdot \vec{d} \right) \pm \sqrt{\left(\vec{e} \cdot \vec{d} \right)^2 - \left(\vec{e} \right)^2 + r^2} \ . \tag{5}$$

If $\Delta = \left(\vec{e} \cdot \vec{d} \right)^2 - \left(\vec{e} \right)^2 + r^2 \geq 0$, it means that the two spheres are in contact, and two solutions f_1 and f_2 are generated. The smallest absolute value is the position when both spheres begin to come in contact, and the largest absolute value is the position when both spheres are out of contact. In order to establish close contact between the spheres, the one that has a small absolute value is selected as the final solution. All reference spheres have corresponding offsets, and the minimum offset is selected as the final position after contact between the target sphere and the reference sphere.

Contacts between the Sphere and the Mould Cavity. As the sphere can be in contact with the inner surface of the cavity, the position of the target sphere must be determined after it moves in the direction $\vec{d}$ and makes contact with the cavity's internal surface. First, the minimum offset is selected as the final location after contact between the target sphere and the cavity surface. When the target sphere is in contact with the lower surface of the mould cavity, the coordinated z-axis value of the adjusted sphere is the actual radius of the target sphere r_m; when the target sphere is in contact with the upper surface of the mould cavity, the coordinated z-axis value of the adjusted sphere is the radius of the current target sphere $h - r_n$, which is the cavity's height h; when the target sphere is in contact with the lateral surface of the cavity, the coordinated position of the x-axis and the y-axis is determined; then, the coordinates can be obtained from the similar triangle relationship as follows:

$$\frac{x_a - x_b}{1} = \frac{y_a - y_b}{\cot \beta} = \frac{z_a - z_b}{\cot \beta / \cos \beta}, \tag{6}$$

where b represents the original position of the target sphere before adjustment; a represents the position of the target sphere after adjustment.

When all spheres are selected as target spheres, and their position is adjusted, the powder particles in the cavity are dynamically adjusted. Repetition several times can make the spheres more consistent and compact.

This article uses a numerical simulation of three-dimensional densification of Cu–Cr powder particles as an example. Specific parameters are set as follows: Cr powder particle diameter is 2 mm, Cu powder particle diameter is 4 mm, cylindrical mould cavity height is 11.3 mm, and the diameter 10 mm. During filling, the two powders are added to the mould cavity at a 1 : 1 ratio [19].

Through the Python interface reserved by MSC Marc software, commands of writing the related mathematical templates are collected in the python source file, and the command line is used to interact with Marc. By operation, 10 coordinate spherical centers with a diameter of 2 and 4 mm are generated in the cylinder, that is, the mould cavity is filled with 10 Cu particles and 10 Cr particles.

Figure 2 is the schematic diagram of the Cu–Cr powder particle pressing structure. In the figure, the Cu–Cr particles are randomized into the film cavity. The upper and lower surfaces of the mould cavity are considered rigid bodies for controlling compression in the y direction of the mold cavity. The 8-node hexahedral element is used to square the powder particles Cu and Cr, with a total of 34,981 grids [20, 21].

Because of the various mechanical properties of Cu and Cr, Cu is easy to deform during combination pressing and a single particle is a complete compact metal. Consequently, Cu is considered an isotropic elastic-plastic material, and Cr is considered an isotropic elastic material. In the elastic–plastic deformation process, the size of the powder particles Cu and Cr is constant [22, 23]. The parameters of the materials used are this: Poisson's ratio $\nu = 0.28$ (Cr) and 0.34 (Cu); elastic modulus $E = 400$ GPa (Cr) and 125 GPa (Cu); yield stress $\sigma_0 = 175$ MPa (Cr) and 70 MPa (Cu).

The formation of powder particles under pressure is a complex problem with nonlinear geometry, contact, and boundary conditions, which belong to the large deformation. Given the solution of complex stress state, according to the assumption of D.C. Drucker: 1) the increase in stress during loading is a positive value; 2) throughout the loading and unloading cycle, when the deformation behavior is purely elastic, and if plastic deformation occurs, the network is positive [24].
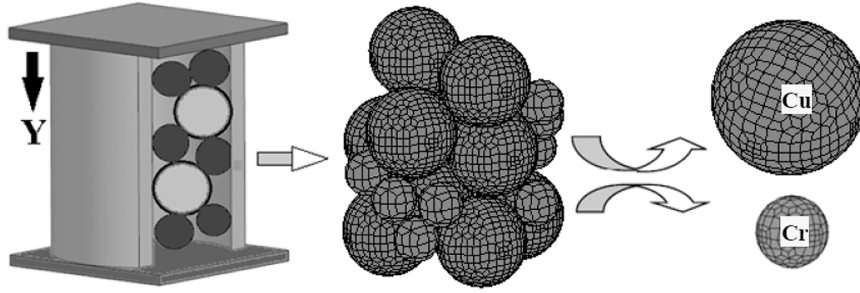
Fig. 2. Schematic diagram of Cu–Cr powder particle compaction structure

In order to further converge residues and adjust the appropriate relaxation factors, the Newton Raphson iteration method is adopted in this article. The contribution of the initial strain to the stiffness is defined as well, the maximum iteration number is 10, and the minimum iteration number is 0. In the contact method, the surface area is chosen as the surface area, the Coulomb bilinear (displacement) is chosen for friction, and the convergence criterion is displacement [25]. The time stage is determined based on the contact movement of the powder particles [26]. The model parameters of the particle contact pattern are as follows: coefficient of restitution is 0.2; coefficient of friction is 0.2; damping coefficient is 0.01; stiffness coefficient is 1.2; contact tolerance deflection factor is 0.9; suppress constant temperature is 800°C.

RESULTS AND ANALYSIS

In order to understand the densification process of Cu–Cr powder particles more clearly, the flow deformation of the particle nodes shall be analyzed. Figures 3*a–f* indicates the total displacement of *y* within the Cu–Cr particles with different time stages.
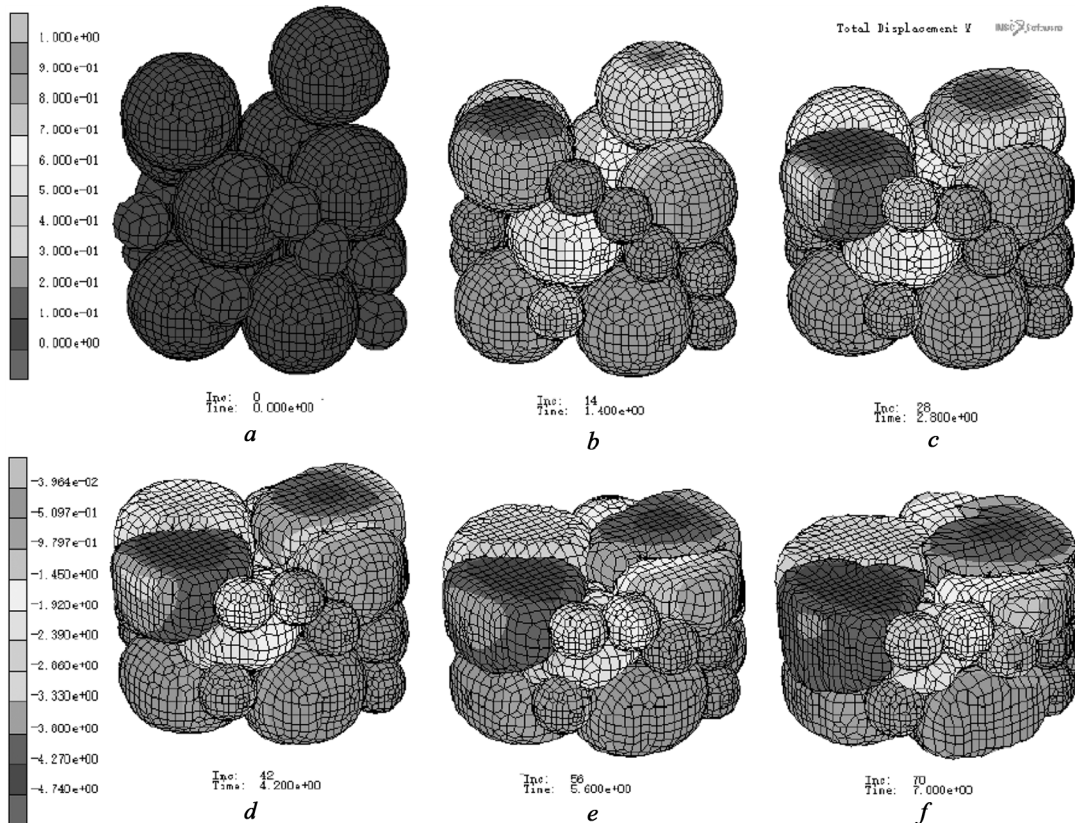

Fig. 3. The *y*-axis displacement of Cu–Cr particles with different time steps: 0 (*a*); 14 (*b*); 28 (*c*); 42 (*d*); 56 (*e*), and 70 (*f*)
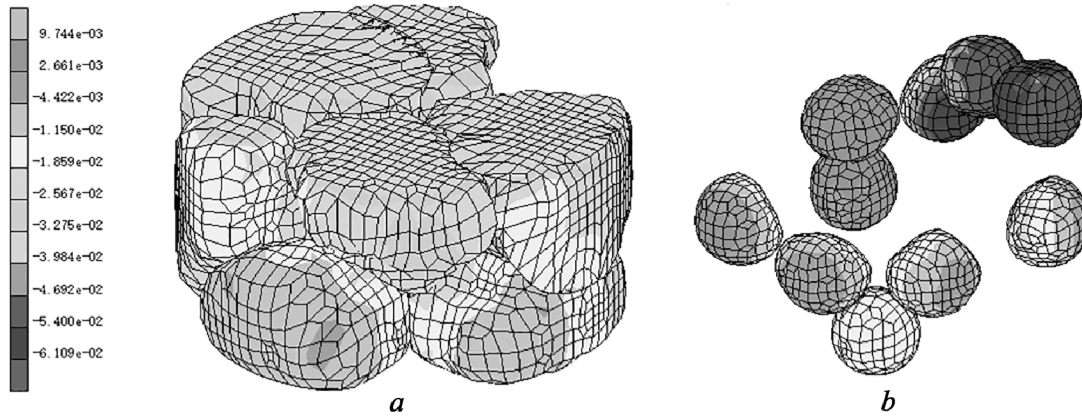
11

Fig. 4. Overall strain cloud diagram of individual Cu (*a*) and Cr (*b*) particles

It can be seen from Fig. 3 that during the initial pressing stage, i.e., when the plastic deformation does not occur, the powder particles in the cavity of the mould flow from top to bottom. The closer the particles are to the mould cavity, the higher the flow velocity, and the entire space has a spiral rotation motion. When compression reaches the yield point, the densified particles undergo plastic deformation, while the Cr particles do not deform when compacted. The results show that space is primarily filled by the deformation of Cu particles. When compaction reaches equilibrium, the particles squeeze one another and move back and forth, gradually tending to equilibrium. However, there are still some differences between the particles.

The main reason is that Cr particles with a higher hardness do not deform, and the deformation of soft Cu particles occurs initially at the point of contact with Cr particles. With the increase of the pressing time stage, the Cu particles spread along the surface of the Cr particles to the surrounding pores and then reach a stable state.

In order to study the straining process of a single particle, the contact between particles and mould wall is selected for analysis (Fig. 3). Figure 4 illustrates the total strain of a particle. Figure 5 shows the strain diagram of the various contact points of the Cu particles.

It can be seen from Figs. 4*a* and *b* that the overall deformation of the Cr powder is not significant, and the overall deformation of the Cu particles is more significant. Consequently, Cu particles are further analyzed.

It can be seen from Figs. 5*a* and *b* that deformation of the Cu powder in contact with the particles occurs first at the point of contact of the particles and then extends inwards along with the point of contact. With the pressing process, the deformation of the particles becomes ever greater. Finally, a concave arc is formed at the point of contact of the round particles, and the deformation of the particles is also concentrated in the concave arc area. For the Cu powder, deformation occurs when one particle contacts both the particle and the mould wall. For powder, deformation occurs first at the point of contact between the particles and the particles and between the particles and the mould wall. The particles and particles extend inside the particles with the points of contact, and the particles and mold walls extend around the mold wall with the points of contact. Finally, concave arcs are formed at the contact points of round particles and particles, and cylindrical arcs are formed at the contact points between particles and mold walls.

In order to better understand the influence of the flux and the law of the Cu–Cr powder particle node on the compactness of the Cu–Cr compound, the spheric coordinates of the powder particles were sampled and labeled. Collection points 1 through 10 are Cu particles, and 11 through 20 are Cr particles. As shown in Fig. 6, the flow path of the Cu–Cr powder particle densification node is shown.

Figure 6*a* is the flow trajectory diagram of the Cu particle node, and Fig. 6*b* is the flow trajectory diagram of the Cr particle node. The figure shows that the trajectory of the nodes in the particles moves upwards and downwards as a whole, and at the same time, there is a trend to turn from the center towards the environment. The downward trend in Cu particles in the initial compaction stage is evident, but the rotational tendency is not significant. The downward movement and rotation of Cu particles at the intermediate stage of compaction are
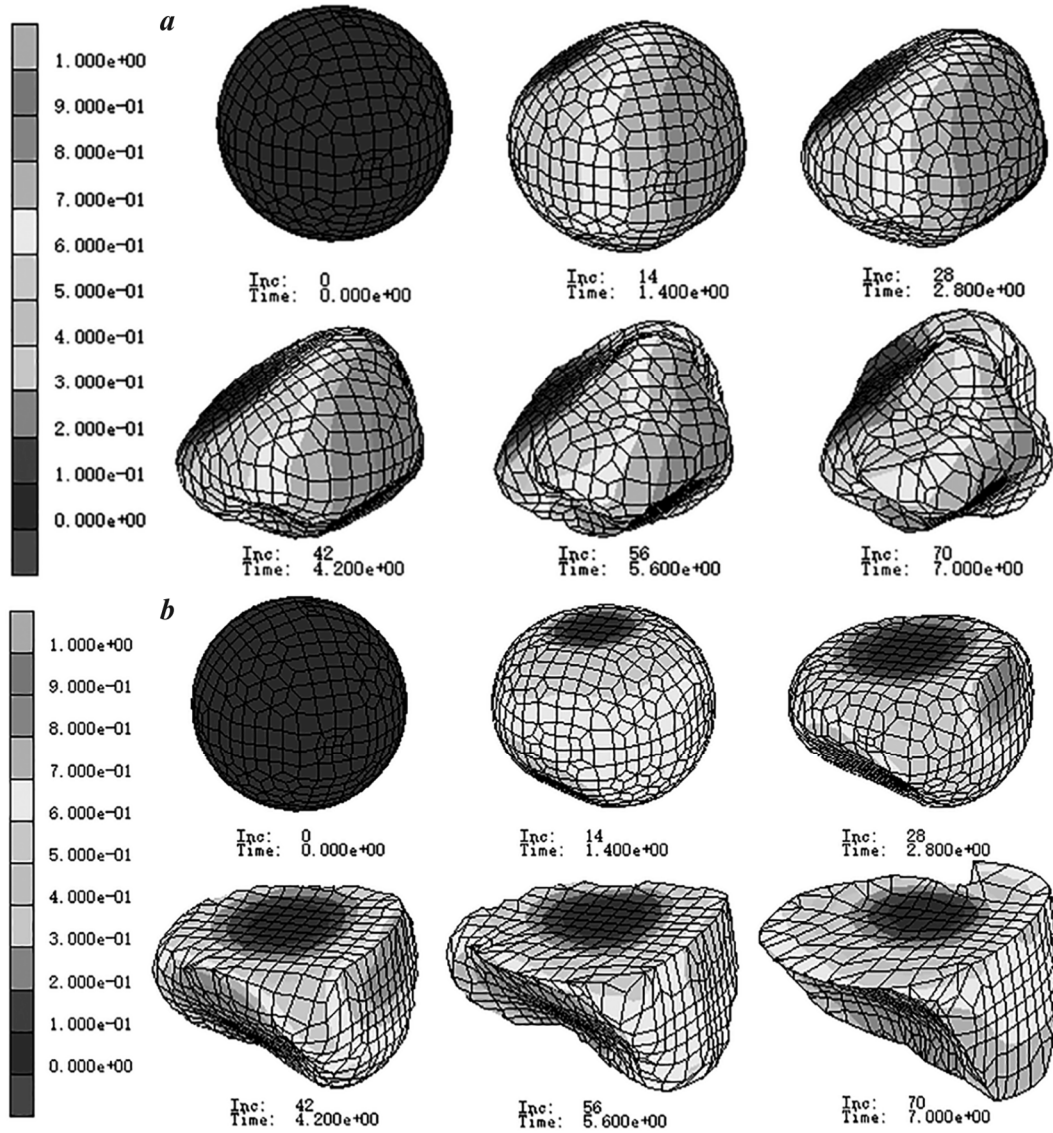
Fig. 5. Deformation diagram of Cu particles at different contact points: *a*) particle-to-particle; *b*) particle-to-particle and the mold wall
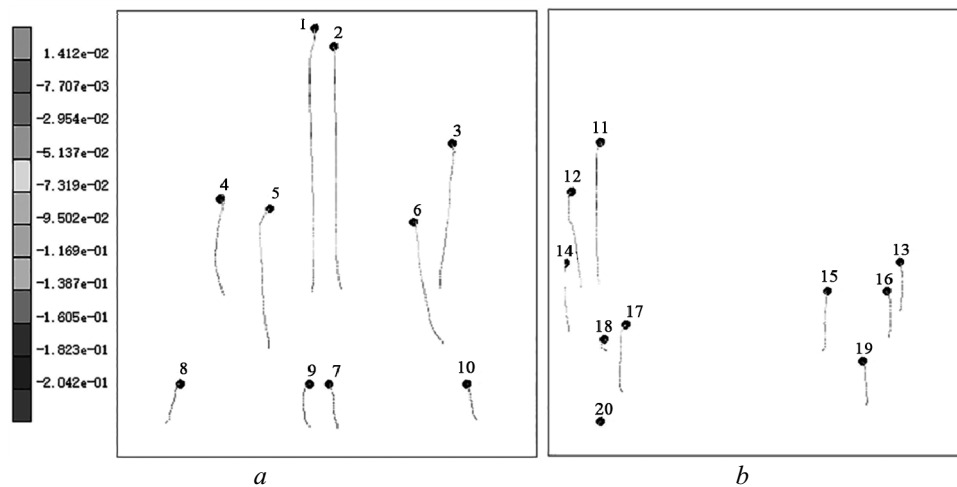

Fig. 6. Flow trajectory diagram of Cu (*a*) and Cr (*b*) powder particle densification nodes

important. The downward trend in Cu particles at the end of compaction is not evident, and the rotation trend is significant. Most Cr particles at the beginning, middle, and end of compaction show an obvious tendency to move and rotate, and only a few of them are not significant.

The nodal pathways of the powder particles Cu and Cr are not coherent, mainly due to low particle deformation at the initial stage of compaction, rearrangement of particles, and lateral sliding. After reorganization is complete, the plastic deformation of the particles occurs mainly, forcing the particles, and the flow of the particle nodes decreases as the density increases.

The relative density of the cavity represents the volume of the particle unit divided by the volume of the cavity. The relative density of the increased pore cavity is equal to 1. This article assumes that the volume of a single Cu and Cr particle remains unchanged as Cu–Cr powder particles are compacted. The initial relative density σ and the relative density after pressing process $\sigma*$ are calculated as follows:

$$\sigma = \frac{10\left(\frac{4}{3}\pi r_1^3 + \frac{4}{3}\pi r_2^3\right)}{\pi\left(\frac{d}{2}\right)^2 h}, \tag{7}$$

$$\sigma* = \frac{10\left(\frac{4}{3}\pi r_1^3 + \frac{4}{3}\pi r_2^3\right)}{\pi\left(\frac{d}{2}\right)^2 (h - h*)}, \tag{8}$$

where r_1 and r_2 are the radius of Cu and Cr particles, accordingly; h and $h*$ are the initial height of the cavity and the pressing displacement, accordingly; d is the cavity diameter.

By integrating the geometric parameters of the model, the original relative density of the cavity can be calculated at 42.48%.

It can be seen from Fig. 7 that with the increase of the time step, the change of the relative density is mainly divided into three sections, and at the initial stage of compacting, the relative density increases linearly. At the intermediate stage of compaction, the velocity of relative density slowly decreases. At the later stage of compaction, the velocity of relative density becomes slower. In fact, at the initial stage of compaction, the Cu and Cr particles undergo mainly an elastic deformation, and the particles move only relatively so that the relative density increases linearly. In the intermediate compaction stage, the particles not only demonstrate an elastic but also a plastic deformation. Motion and rotation of particles occur simultaneously, and plastic deformation slows down the compaction rate. At the later stage of compaction, only plastic deformation and particle rotation occur, making the relative density velocity the lowest. Therefore, in practical application, the particles can be pressed closer, and the
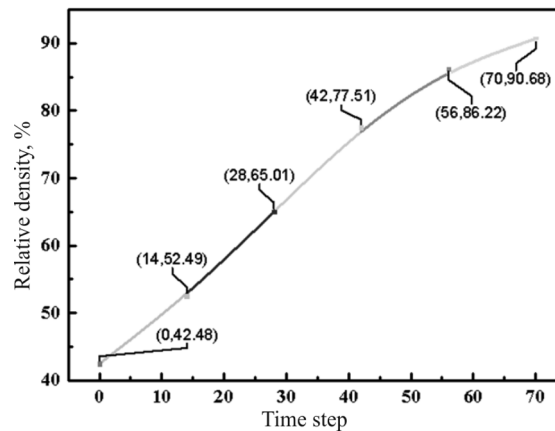

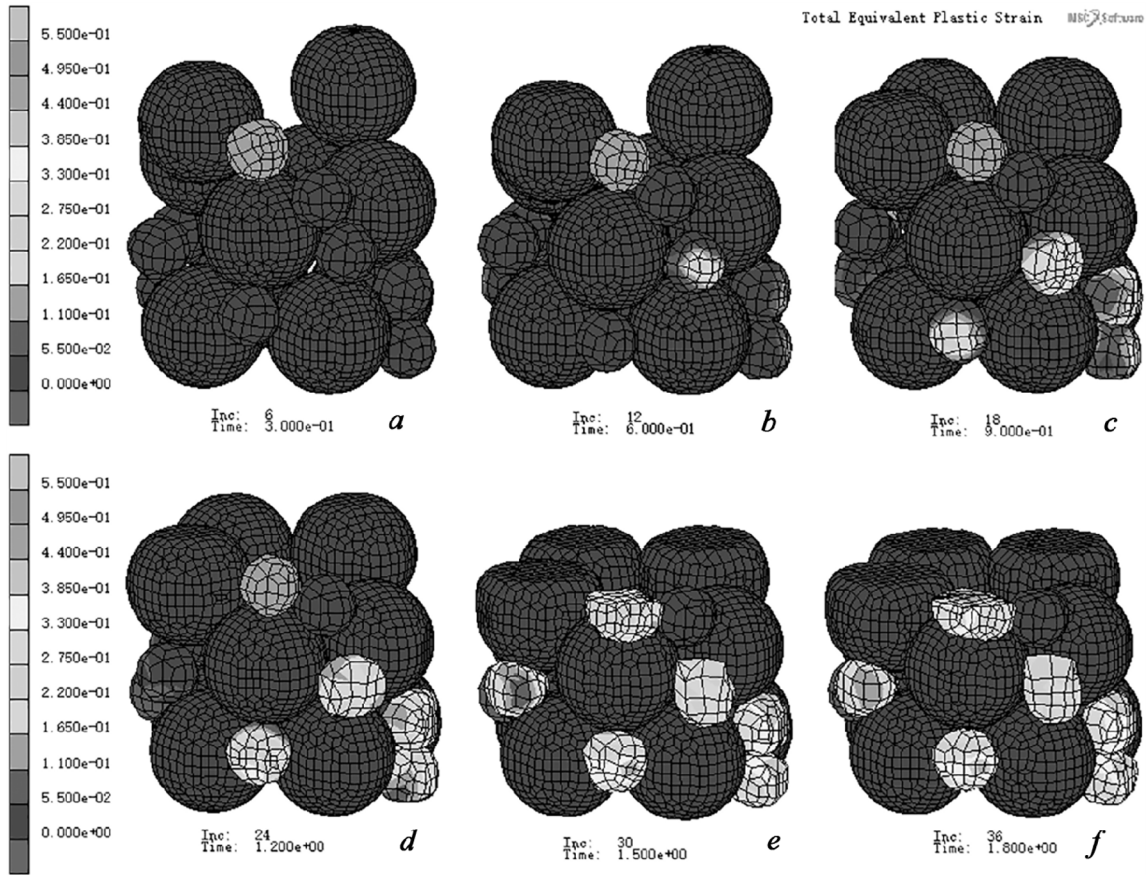*Fig. 7.* Relative density vs. time step

Fig. 8. Total equivalent plastic strain: time step 0 (*a*); 14 (*b*); 28 (*c*); 42 (*d*); 56 (*e*); 70 (*f*)

density of the products can be improved by changing the size of the pressing speed and by adopting the sectional pressing method.

This article aims to further analyze and discuss the process of pressing Cu and Cr randomly arranged powder particles. The exchange between the powder and particle materials in the three-dimensional model was established. A cloud map of the overall displacement change of the three-dimensional particle was obtained as shown in Fig. 8.

It can be seen from Fig. 8 that the deformation of powder particles can be divided into the following three stages: the primary stage of mild deformation, the main stage of severe deformation, and the stage where the strain tends to stabilize.

In the initial stage of mild deformation, the deformation of the Cu particle, the flow path of the particles, and the law of deformation of a particle comply with the law of analysis above. The same applies to Cr particles. However, individual deformation of the Cu particles is lower than that of the preceding large particles, and individual deformation of the Cr particles is higher than that of the preceding small particles. It can be attributed to the size of the particles themselves, i.e., the bigger the powder particles, the greater the degree of deformation during the compression process.

The final relative density of the compaction model is 85.48% and is lower than the original model. It can be seen that a relatively mild material can be selected for large particles to obtain a higher density in the process of heterogeneous compaction of powder particles of not equal diameter.

The temperature in the press mold cavity, the initial temperature of the particles, and the heat generated by the extrusion friction will all affect densification [27]. Assuming that the pressing process is at a constant temperature, the influence of temperature on the relative density after pressing is investigated. Figure 9 displays the relative density variation curve for Cu–Cr particles at each constant temperature.
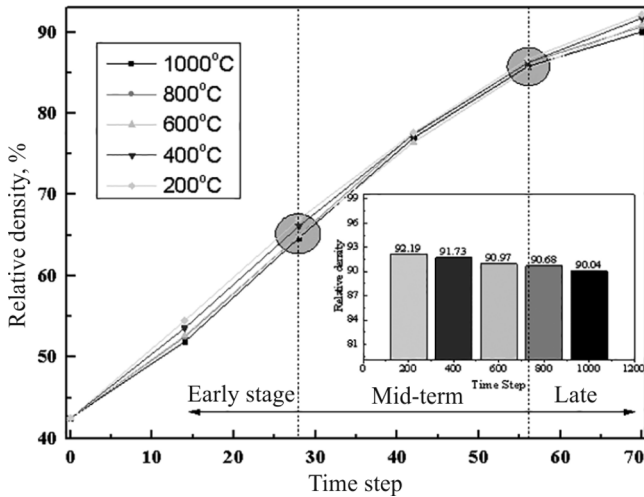
15

Fig. 9. Change curve of relative density in Cu–Cr particles at various constant temperatures
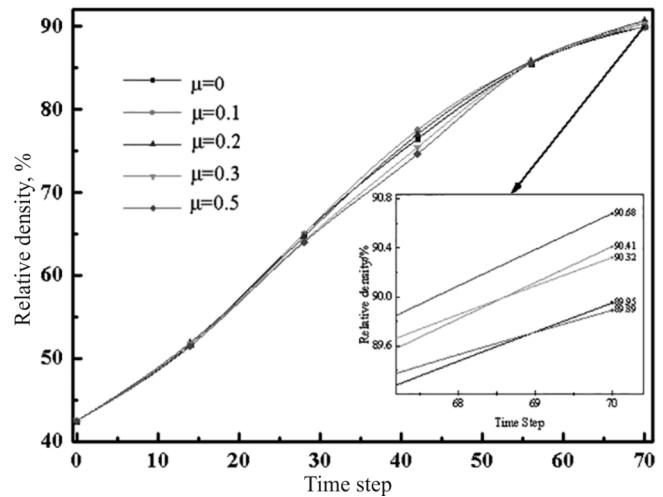

Fig. 10. The effect of friction coefficient on the Cu–Cr particles densification process

It can be seen from Fig. 9 that the greater the temperature, the lower the relative density. With a temperature of 200°C, the relative density is 92.19%. When the temperature is 1000°C, the relative density increases to 90.68%, a difference of 1.51%. This is because Cu–Cr particles and the mould cavity undergo thermal expansion into a high-temperature environment, and the internal friction of the extrusion force decreases the density of Cu–Cr particles as the temperature increases.

Since the lubricating material has a major influence on the pressing result, other parameters are monitored unchanged during the Cu–Cr particles densification. Different friction coefficients are used to simulate the pressing process and analyze the effect of the friction coefficient on the relative density [28]. To simplify the calculation and study the significant effect of the coefficient of friction μ on the Cu–Cr particle densification process, the coefficient of friction between the particles and the wall of the die is fixed at various fixed values.

It can be seen from Fig. 10 the relative density after pressing is 89.79%, provided no friction is present. When the friction coefficient is 0.2, the relative density after pressing is the highest, 90.684%, which is 0.89% above the coefficient without friction. The analysis shows that the smaller the coefficient of friction, the ultimate density is not necessarily greater. The coefficient of friction has an evident effect on the medium-term densification of Cu–Cr particles, and the effect is low in early and late stages. As friction increases, so does the relative density during pressing. After attaining a certain value, as the friction force increases, the relative density of compaction decreases. As a result, a proper adjustment of the friction coefficient can make Cu–Cr particles more adjusted and improve density.

COMPARISON OF EXPERIMENT AND SIMULATION RESULTS

In order to verify the accuracy of the simulation results, this experiment relies on the experimental equipment platform of the Zhuzhou melting group to verify the model system. Metal particles of Cu (400 μm) and Cr (200 μm) were mixed and charged at the 1 : 1 ratio. After vacuum degassing, they were placed in the die chamber of the QIH-15 press for compaction. Figure 11 shows the experiment sample and equipment.

The experimental parameters of the pressing process are a constant temperature of 800°C, a pressing force of 160 MPa, and a unidirectional pressing. The comparison of the data to the simulation results is presented in Table 1. The comparative analysis of 5 experiments and simulation results suggests that once the experiment is completed under the same pressing conditions, in accordance with the density test standard GB/T3850-1983, measured by the Archimedes method, the mean experimental density will be 91.29%. As a result, the average density was 90.24%, and the relative error was 1.05%. There is some variation between the experiment and the simulation results because the friction coefficient value in the simulation parameters is constant, while the friction coefficient over the

Fig. 11. Experimental samples (*a*) and equipment (*b*)

TABLE 1. Comparison of Experiment and Simulation Results for Cu–Cr Powder Particle Densification (%)

Density results	Repeat No.					
	1	2	3	4	5	Average value, %
Experiment	91.33	92.43	89.73	90.87	92.33	
	91.02	92.67	89.92	91.11	92.68	91.29
	91.34	92.12	89.24	89.87	92.74	
Simulation	90.66	90.45	89.98	89.95	90.44	
	90.25	90.03	89.87	89.98	90.84	90.24
	90.54	90.35	90.23	89.43	90.56	

experiment varies. There are two sides to friction in the extrusion process. Friction between the particles and the matrix wall does not enhance the density and surface quality of the Cu–Cr powder, whereas friction between particles is conducive to close adhesion between powder particles.

CONCLUSIONS

This article establishes a mathematical model of the random accumulation of Cu–Cr powder particles in the mould cavity using a computational programming language and studies the binary powder particles and nodes inside the particles during the unidirectional pressing process. The following conclusions can be drawn.

In the initial compression stage, the powder particles in the cavity flow up and down in general, showing a spiral rotational movement in space. When compression reaches the yield point, Cr particles do not deform during compression. The gap between the particles is mostly filled by the deformation of the Cu particles. When compression reaches a steady state, the particles squeeze together to produce a small reciprocating motion and gradually become stable, but there are still some differences between the particles; the Cu powder with a particle-to-particle contact expands inwardly with the point of contact, and eventually forms a concave arc at the point of contact of the round particle; the contact point between the Cu powder particles and mould wall expands inwards from the particle, and the particle and mould wall shall extend with the point of contact to the periphery of the mould wall; finally, a concave arc occurs at the point of contact between the round particle and the particle, and a cylindrical arc is formed at the contact between the particle and the mould wall.

The results show that the nodal path in the powder particles moves up and down, and there is a tendency to rotate from the center to the surrounding areas; Cu particles in the early compaction zone exhibit an evident

downward trend, but the rotational tendency is not significant; the downward movement and rotation tendency of the Cu particles at the intermediate compaction stage are significant; the downward movement of Cu particles in the late compaction zone is not evident, and the rotation tendency is not significant. Most Cr particles at the beginning, middle, and end of compaction show an obvious tendency to move and rotate, and only a few of them are not significant.

In the powder densification process, i.e., the larger the powder particles, the higher the deformation during the pressing deformation process; the higher the temperature in the mould cavity, the smaller the relative density, the higher the friction in the cavity, the higher the pressure. The greater the relative density, but after reaching a certain value, the lower the relative density of the pressing.

REFERENCES

1. B. Harthong, D. Imbault, and P. Doremus, "The study of relations between loading history and yield surfaces in powder materials using discrete finite element simulations," *J. Mechan. Phys. Sol.* **60**, No. 4, 784–801 (2012).

2. M.C. Zhou, S.Y. Huang, J.H. Hu, Y. Lei, F.L. Zou, S.W. Yan, and M. Yang, "Experiment and finite element analysis of compaction densification mechanism of Ag–Cu–Sn–In mixed metal powder," *Powder Technol.*, **313**, 68–81 (2017).

3. C.V. Nguyen, Y. Deng, A. Bezold, and C. Broeckmann, "A combined model to simulate the powder densification and shape changes during hot isostatic pressing," *Computer Methods Appl. Mechan. Eng.*, **315**, 302–315 (2016).

4. T. Watanabe, A. Yanagisawa, and T. Sasaki, "Development of Ag based brazing filler metal with low melting point," *Sci. Technol. Welding Joining*, **16**, No. 6, 502–508 (2011).

5. J. Ai, J.F. Chen, J.M. Rotter, and J.Y. Ooi, "Assessment of rolling resistance models in discrete element simulations," *Powder Technol.*, **206**, No. 3, 269–282 (2011).

6. D.F. Wang, *Characterization of Radical Microscopic Properties of Orderly Packed Structure of Binary Spherical Particles* [in Chinese], Northeastern University (2014), pp. 1–83.

7. Y.X. Zhang, *Multi-Particle Finite Element Simulation of Particle Micro-Behavior during Powder Compaction* [in Chinese], Northeastern University (2015), pp. 1–78.

8. C. Li, *Experimental Study on One-Dimensional and Three-Dimensional Vibration Packing Densification of Binary Size Balls* [in Chinese], Northeastern University (2011), pp. 1–119.

9. D.W. Wolla, M.J. Davidson, and A.K. Khanra, "Prediction of ductile fracture initiation for powder metallurgical aluminum-copper preforms using FEM," *Int. J. Mechan. Mater. Eng.*, **10**, No. 1, 8 (2015); https://doi.org/10.1186/s40712-015-0036-9

10. Y. Zhang and F.Z. Wang, "Numerical simulation of effects of pressure on densification of hot isostatic pressing of CuCr25 powder" [in Chinese], *Hot Working Technol.*, **47**, No. 2, 76–85 (2018).

11. S. Zhao, F.Z. Wang, and D.Q. Ou, "Simulation of heterogeneous powder compression deformation behavior of Cu–W" [in Chinese], *Ordnance Mater. Sci. Eng.*, **41**, No. 2, 58–62 (2018).

12. H.P. Chen and F.Z. Wang, "Finite element simulation of hot isostatic pressing densification process for W–Cu alloy powder" [in Chinese], *Mater. Mechan. Eng.*, **41**, No. 6, 69–74 (2017).

13. Q.X. Liu, F.Z. Wang, Y. Zhang, and H.P. Chen, "Numerical simulation of macro segregation and temperature field of Cu–Cr two binary alloy" [in Chinese], *Mater. Sci. Technol.*, **24**, No. 6, 73–78 (2016).

14. Y.B. Wang, F.Z. Wang, Y.K. Wang, Y.F. Li, and W.G. Du, "Three-dimensional numerical simulation of deformation and particle flow of Cu–Cr powder densified particles" [in Chinese], *Acta Mater. Compos. Sinica.*, **36**, No. 12, 2902–2911 (2019).

15. D.G. Wang, Y.C. Wu, and M.H. Jiao, "Research and simulation of influence of three-axial compaction on powder metallurgic products properties," *Acta Metall. Sinica* (English Letters), **21**, No. 2, 116–124 (2009).

16. Y.X. Zhang, X.Z. An, and Y.L. Zhang, "Multi-particle FEM modeling on microscopic behavior of 2D particle compaction," *Appl. Phys. A*, **118**, No. 3, 1015–1021 (2015).

17. A.J. Taleghanim, M.R. Navase, M. Salehi, and J.M. Torralba, "Hot deformation behaviour and flow stress prediction of 7075 aluminium alloy powder compacts during compression at elevated temperatures," *Mater. Sci. Eng. A*, **534**, No. 2, 624–631 (2012).

18. B. Guo, J. Ao, Y. Xu, and Z.J. Zhang, "Constitutive equation for the flow and densification behaviors of powder metallurgy Fe–0.5C–2Cu steel at elevated temperatures," *Steel Research Int.*, **88**, 22–31 (2017).

19. C. Feng, D.D. Sun, and H.S. Chen, *New Marc Example Tutorial and Common Problem Analysis* [in Chinese], China Water & Power Press, Beijing (2016), pp. 225–229.

20. D.F. Khan, H. Yin, Z. Usman, M. Khan, X.J. Yuan, W.H. Wang, and X.H. Qu, "Improvement of a high velocity compaction technique for iron powder," *Acta Metal Lurgica Sinica* (English Letters), **26**, No. 4, 399–403 (2013).

21. A.V. Kuzmov, M.B. Shtern, and O.G. Kirkova, "Effect of billet elongation degree and strain hardening of the powder on compaction with rotating die," *Mathematical Models and Computing Experiment in Material Science: Collected Papers* [in Russian], **21**, 101–108 (2019).

22. C.V. Nguyen, Y. Deng, A. Bezold, and C. Broeckmann, "A combined model to simulate the powder densification and shape changes during hot isostatic pressing," *Computer Methods Appl. Mechan. Eng.*, **315**, 302–315 (2016).

23. D.C. Tsai and W.S. Hwang, "Numerical simulation of solidification morphologies of Cu–0.6 Cr casting alloy using modified cellular automaton model," *Trans. Nonferrous Met. Soc. China*, **20**, No. 6, 1072–1077 (2010).

24. B.Y. Xu, *Plastic Echanics* [in Chinese], Higher Education Press, Beijing (1988), pp. 88–111.

25. J. Paul, S. Romeis, P. Herre, and W. Peukert, "Deformation behavior of micron-sized polycrystalline gold particles studied by in situ compression experiments and frictional finite element simulation," *Powder Technol.*, **286**, 706–715 (2015).

26. F. Güner, Ö.N. Cora, and H. Sofuoglu, "Effects of friction models on the compaction behavior of copper powder," *Tribol. Int.*, **122**, 125–132 (2018).

27. K.M. Arndt, S. Aman, R. Fuchs, and J. Tomas, "Contact properties determination of macroscopic fine disperse glass particle via compression tests in normal direction," *Adv. Powder Technol.*, **28**, 101–114 (2017).

28. M.H. Jiao, L. Sun, M. Gu, D.G. Wang, and Y.C. Wu, "Mesoscopic simulation of the compression deformation process of powder particles," *Adv. Mater. Research.*, **38**, No. 5, 169–173 (2013).